Experiments on turbulent-flow phenomena in eccentric annular ducts

By V. K. JONSSON AND E. M. SPARROW

University of Minnesota, Minneapolis, Minnesota

The investigation to be described here is a wide-ranging experimental study aimed at determining both the details of the flow field and the pressure drop and friction factor characteristics for turbulent flow in eccentric annular ducts. The experiments were performed utilizing three annular ducts of different diameter ratios; in each case the eccentricity was varied from zero (concentric annulus) to unity (walls in contact). To provide the broadest possible perspective, the measurements of the velocity field are presented in three different ways. First, contour maps showing lines of constant velocity are constructed. From these are deduced circumferential distributions of the local shear stress on the bounding walls. Velocity profiles along lines normal to the walls are represented in terms of both law-of-the-wall variables and defect-law variables. Neither of these representations affords complete agreement with the universal circular-tube distributions. In general, the defect law provides a somewhat closer correlation of the results for the eccentric annulus with those for the tube. The experimental findings do not substantiate a prior analytical model which assumes that the universal law of the wall applies on all lines normal to the bounding walls of the annulus. Friction factors, based on static pressure measurements, are shown to decrease with increasing eccentricity. The measured friction factors are in fair agreement with those of analysis. Hydrodynamic development lengths, deduced from entrance-region pressure data, are found to increase with increasing eccentricity. Circumferential pressure variations also increase with eccentricity.

1. Introduction

In most internal flow problems of practical interest, the velocity field is turbulent. Even for circular tubes, the mechanism of turbulent transport is by no means fully understood although various semi-empirical analytical models have been successfully employed for predicting the velocity distribution and the pressure drop. For non-circular ducts, where the transport phenomena are intrinsically more complex, the formulation of an analytical model is marked by correspondingly greater uncertainties. Consequently, it remains for experiment to provide fundamental information on the turbulent flow field in such ducts.

The particular non-circular duct configuration of interest here is the eccentric annulus. This is a report of a wide-ranging experimental investigation of the fluid flow characteristics of such ducts. Consideration is given to both overall quantities, such as the pressure drop and the friction factor, and to flow field

details, such as the velocity distribution and the circumferential distribution of the shear stress on the bounding walls. The velocity field is presented on contour maps and in terms of both law-of-the-wall variables and defect-law variables, the latter representations permitting comparisons with conventional semi-empirical turbulent-flow models. The major emphasis of the investigation was centred on the condition of hydrodynamically developed flow. However, pressure-drop measurements were also made in the hydrodynamic entrance region, and inlet lengths were deduced. Consideration was also given to circumferential pressure variations.

The experiments were conducted with air as the working fluid. Annular ducts having three different diameter ratios were employed, $d_1/d_2 = 0.281$, 0.561, and 0.750 (subscript 1 refers to the inner bounding wall and subscript 2 to the outer bounding wall). For each of these ducts, the eccentricity was varied from zero (concentric annulus) to unity (walls in contact). The Reynolds-number range of the investigation extended from 18,000 to 180,000. Further details of the experimental apparatus are to be given later.

From a review of the literature, it is evident that only sparse prior investigation has been accorded to turbulent flow in eccentric annular ducts. An analysis of the problem was performed by Deissler & Taylor (1955). In the analytical model, it was assumed that the universal velocity profile for circular tubes, expressed in law-of-the-wall variables, can be applied along lines normal to the bounding walls of the annular duct. In order to determine the actual velocity distribution on the basis of the aforementioned model, it is necessary to solve for the circumferential distribution of the wall shear stress. The shear distribution was obtained from a lengthy, graphical trial-and-error procedure. As a matter of interest, it may be noted that the same model was employed by Deissler & Taylor in studying other non-circular duct flows.

An experimental determination of fully-developed friction factors for a narrow range of relatively large diameter-ratio ducts ($d_1/d_2 = 0.688$, 0.750, 0.875) is reported by Dodge (1963). All the data were collected using a single pair of pressure taps. Such a measurement technique may well lead to uncertainties if there are local irregularities in the geometry of either tap. Furthermore, for some of the test conditions, it is not certain that hydrodynamically developed conditions prevailed at the pressure tap locations. Wolffe (1962) measured velocity profiles along lines perpendicular to the outer bounding wall in an annulus with diameter ratio 0.65 and eccentricity 0.46. Inasmuch as the flow field was determined for only a single test condition, conclusions as to the validity of the Deissler–Taylor model cannot be drawn.

Prior studies of turbulent flow in concentric annuli, although not of immediate relevance to this presentation, have been surveyed by the authors. For brevity this survey is not included here; it may be found, however, in the thesis of Jonsson (1965) from which this paper is drawn.

2. The experimental apparatus

The investigation was carried out utilizing an open-circuit flow system. Filtered air, supplied by a centrifugal compressor, was metered by either of two specially

calibrated orifices and then delivered to a plenum chamber. A uniform distribution of flow at the exit of the plenum was achieved by employing a baffling arrangement plus 100 layers of metal lathe screening. The uniformity of the flow was verified by measurement.

From the plenum, the airstream passed into the test section, which consisted of an outer tube of 4·008 in. inside diameter, and any one of three interchangeable inner tubes, whose outside diameters were 3·004, 2·248, and 1·124 in. The corresponding diameter ratios, d_1/d_2, were 0·750, 0·561, and 0·281. The tubes had been carefully selected for straightness and uniformity of diameter. The test section and plenum were constructed so that there was a sharp-edge hydrodynamic inlet condition at the outer tube. On the other hand, the inner tube extended back into the plenum, where it was supported.

The test section was 20 ft. long and was oriented vertically to eliminate the possibility of sag. In terms of the hydraulic diameter, the lengths of the three annular ducts were 232, 132, and 81, respectively. The dimensions of the test section were selected to provide ample cross-sectional space for performing probe measurements and ample axial length to ensure hydrodynamic development of the flow. In connexion with the flow development, cognizance was taken of the possibility that the length needed to achieve fully-developed conditions would be greater in a non-symmetric flow field. At the downstream end of the test section, the airstream passed out into the laboratory room.

The outer tube was rigidly anchored at both ends. On the other hand, the inner tube could be moved sideways relative to the outer tube. In this way, any eccentricity between zero (concentric cylinders) and unity (cylinders in contact) was achievable. The distance between the bounding walls was measured at four circumferential locations, at each of three axial stations (near the inlet, midway along the length, and near the exit). These measurements were made by inserting a depth micrometer into suitable access holes in the wall of the outer tube. On this basis, the distance between the tubes was known to within 0·002 in.

Static pressure information was obtained from 42 pressure taps located both longitudinally and circumferentially on the outer tube. The taps were situated at 23 axial stations. The holes were produced by an 'electrode' drill which consisted of a 0·032 in. carbon steel tube that acted as an anode; the duct wall acted as cathode. Preliminary tests had demonstrated that holes produced in this way were far freer of burrs than were holes drilled by conventional mechanical methods. In addition, as a further precaution, the outer tube was internally honed throughout its length.

The longitudinal distribution of static pressure was displayed on a glass-tube manometer bank. The heights of the manometer fluid in the various tubes were read with a Gaertner cathetometer capable of discriminating 0·005 cm (0·002 in.) in the range from 0 to 100 cm. The circumferential variation of static pressure at a given axial station was read from a Merriam micromanometer which could discriminate differences of 0·001 in. of the manometer fluid.

The details of the velocity field were measured in a cross-section 3 in. from the duct exit. For this purpose, either of two total pressure probes was employed.

one with a round tip and the other with a flattened tip. Both probes were fabricated from stainless steel hypodermic tubing. For the flattened probe, the tip was drawn to a wall thickness of 0·0025 in. and then flattened to a 0·004 by 0·040 in. opening and honed smooth. The round-tip probe had a 0·010 in. diameter opening with 0·004 in. wall thickness.

The impact probe was mounted on a specially designed traversing mechanism which permitted carefully controlled travel normal to either bounding wall at any circumferential location. The movement of the probe normal to the wall was regulated by an advancing screw with a dial calibrated to 0·001 in. Contact of the probe with the wall was detected by electrical continuity. The impact pressure sensed by the probe was read with a Gaertner 4 in. range cathetometer capable of discriminating to ±0·0001 in.

Various details of the test apparatus have been omitted here in the interests of concise presentation. Further information is available in Jonsson (1965).

3. Presentation of results

The information that may be of most immediate practical interest is that of the pressure drop and friction factor results. These are presented in the subsequent paragraphs. Next, the circumferential distributions of the local wall shear stress, as deduced from velocity measurements, are described and discussed. In later sections of the paper, the details of the flow field are displayed in several ways. Lastly, information pertaining to the hydrodynamic entrance region and to circumferential pressure variations is given.

4. Pressure drop, friction factor, and local wall shear distribution

4.1. *Pressure drop and friction factor*

The measured longitudinal distribution of static pressure was rephrased as a distribution of the longitudinal pressure gradient dp/dz. This was accomplished by fitting second-degree, least-squares polynomials through five successive points and differentiating at the mid-point. The pressure gradients thus derived provide interesting information for the hydrodynamic-development region as well as for the region of fully-developed flow. At this point in the presentation, attention will be given to the latter.

The existence of the fully-developed régime is identified by the constancy of the pressure gradient. Depending upon the hydraulic diameters of the various ducts, from six to twelve pressure-tap locations fell within the fully-developed régime. A least-squares straight line was fitted through the fully-developed static-pressure values. As an indication of the remarkable absence of scatter, it may be noted that the standard deviation of the points was no more than 0·5 % relative to the least-squares value.

The fully-developed friction factor can be obtained from the equation of definition; that is

$$f = (-dp/dz)\, d_h / \tfrac{1}{2}\rho u_b^2, \quad d_h = d_2 - d_1. \tag{1}$$

Furthermore, a force balance extended over the cross-section yields

$$\pi(d_1 + d_2)\,\bar{\tau} = \tfrac{1}{4}\pi(d_2^2 - d_1^2)\,(-dp/dz), \tag{2}$$

in which $\bar{\tau}$ is the shear stress averaged along *both* bounding walls. Upon combining (1) and (2), an alternative expression for f results

$$f = 4\bar{\tau}/\tfrac{1}{2}\rho u_b^2. \tag{3}$$

The friction-factor information obtained by evaluating (1) has been correlated by a power-law relationship of the type $f = C/Re^n$, where Re is the Reynolds
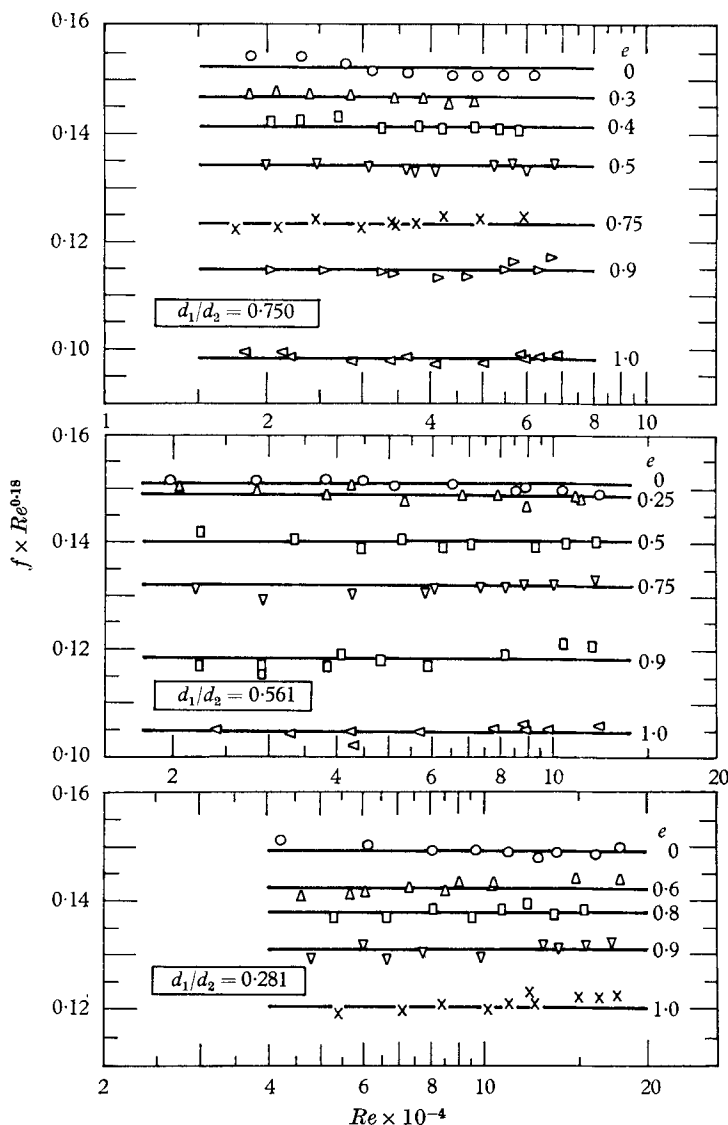

FIGURE 1. Friction factor results for annular ducts.

number based on the hydraulic diameter. By careful analysis of the results, it was found that an n value of 0·18 provided the most satisfactory correlation for all Reynolds numbers, diameter ratios, and eccentricities.

The friction-factor results are presented in figure 1. The figure is divided into three separate parts, each representing a different diameter ratio. Horizontal

lines have been passed through points corresponding to a fixed eccentricity.† From the ordinate values of these lines, the constant C of the correlation $f = C/Re^{0.18}$ can be read directly. From a study of the figure, it is seen that for some cases there is a slight systematic departure of the points from the corresponding horizontal line. This indicates that a Reynolds-number exponent slightly different from 0·18 is appropriate for that case. However, these deviations are very small. In fact, in no instance is the deviation between the data points and the correlation line greater than 2 %. In general, the deviations are much smaller.
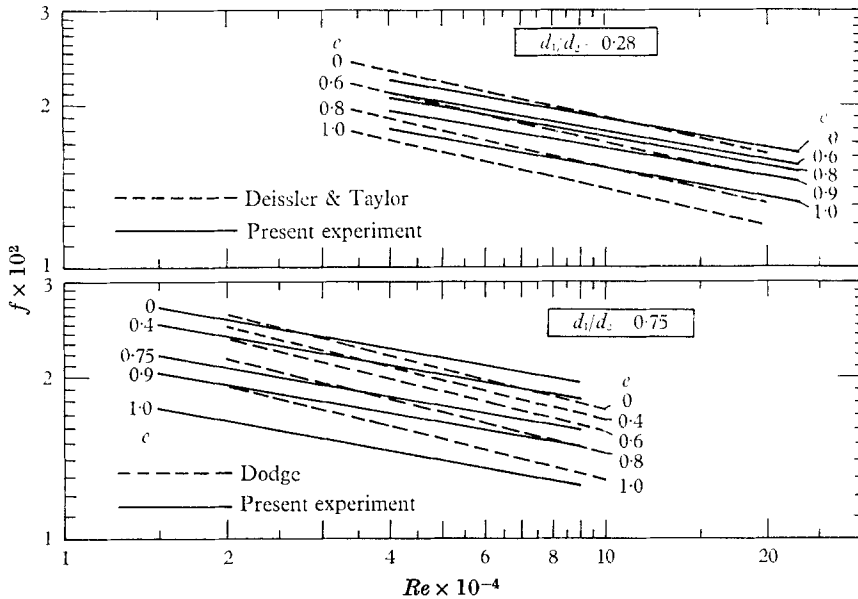

FIGURE 2. Comparisons of friction factor results.

Further inspection of the figure reveals that for a fixed diameter ratio and Reynolds number, the friction factor decreases with increasing eccentricity. This trend is accentuated as the duct diameter ratio increases toward unity. Furthermore, at a fixed eccentricity and Reynolds number, f decreases as d_1/d_2 increases at intermediate and large eccentricities. For the concentric case there is a slight opposite trend.

The experimentally determined friction factors may be compared with those of the Deissler–Taylor analysis, the latter being available for the diameter ratio of 0·281. The comparison is shown in the upper graph of figure 2, where the data points are omitted to preserve clarity. The results for the concentric case show good agreement. However, with increasing eccentricity, the deviation between experiment and analysis becomes more pronounced, the analytical results generally falling low. The maximum deviation is of the order of 15 %. In view of the departures (to be described later) of the analytically postulated flow field

† The eccentricity e is a dimensionless representation of the distance s between the centres of the tubes, the reference length being $(r_2 - r_1)$.

from that actually measured, the level of agreement shown in figure 2 is surprisingly good.

The lower portion of figure 2 contains a comparison of the experimentally determined friction factors of Dodge with those of this investigation. Dodge found no effect of diameter ratio in the range $0 \cdot 688 \leqslant d_1/d_2 \leqslant 0 \cdot 875$. Consequently, his results are presented with the present ones for $d_1/d_2 = 0 \cdot 750$. The data points are once again omitted for the sake of clarity. The agreement between the two experiments is only fair, the largest deviation being of the order of 15 %. As discussed in §1, the results of Dodge are of uncertain accuracy owing to matters of experimental technique.

Mention may be made of certain preliminary tests carried out as part of this investigation. In an altogether different apparatus and with water as the working fluid, fully-developed friction factors were determined for the case $d_1/d_2 = 0 \cdot 5$, $e = 0 \cdot 9$. The data points from these runs were in excellent agreement with the air data shown in figure 1 $(d_1/d_2 = 0 \cdot 5, e = 0 \cdot 9)$.

4.2. *Circumferential variation of wall shear stress*

The distribution of the local shear stress on the bounding walls was deduced from the detailed measurements of the flow field. The actual determination of the local wall shear was accomplished with the aid of velocity contour diagrams that were constructed from the flow measurements. In anticipation of later results, attention may be briefly focused on figure $4(a)$ or (b), where representative contour diagrams are presented. On any one of the contour diagrams, the solid lines represent lines of constant velocity (isovels). The broken lines appearing in the contour diagrams are gradient lines; these have been constructed perpendicular to the isovels. In a fully-developed unidirectional flow, the gradient lines are also lines of zero shear. The dividing gradient line subdivides the flow into two regions, an inner region and an outer region.†

The local wall shear stress can be found by making a force balance on a control surface bounded by two adjacent gradient lines, the dividing gradient line, and the wall. If ΔA denotes the cross-sectional area thus enclosed and ΔL is the length of the corresponding arc on the bounding wall, then one can write

$$\tau = \frac{\Delta A}{\Delta L} \left(-\frac{dp}{dz} \right). \tag{4}$$

Such a force balance applies for fully-developed, unidirectional flow. The area ΔA was measured by a planimeter and the arc length ΔL by a protractor; $(-dp/dz)$ is the fully-developed pressure gradient. The shear stress thus obtained was assigned to the mid-point of the arc.

The local shear stress distribution on the inner bounding wall is denoted by $\tau_1(\theta_1)$, while the corresponding distribution on the outer bounding wall is denoted by $\tau_2(\theta_2)$. θ_1 and θ_2 are the respective angular co-ordinates on the inner

† The extremities of the dividing gradient line pass through the points of maximum velocity in the largest and smallest gaps.

and outer walls. If $\bar{\tau}_1$ and $\bar{\tau}_2$ respectively designate the circumferential averages of $\tau_1(\theta_1)$ and $\tau_2(\theta_2)$, an overall force balance yields

$$\frac{r_1}{r_1+r_2}\frac{\bar{\tau}_1}{\bar{\tau}}+\frac{r_2}{r_1+r_2}\frac{\bar{\tau}_2}{\bar{\tau}} = 1, \tag{5}$$

in which $\bar{\tau}$ is the overall average shear stress discussed in connexion with equation (2). The foregoing suggests a dimensionless representation of the local wall shear results in terms of the parameters

$$\frac{r_1}{r_1+r_2}\frac{\tau_1(\theta_1)}{\bar{\tau}} \quad \text{and} \quad \frac{r_2}{r_1+r_2}\frac{\tau_2(\theta_2)}{\bar{\tau}}. \tag{6}$$

Such a representation was shown to have the particular virtue of being independent of the Reynolds number within the range investigated.
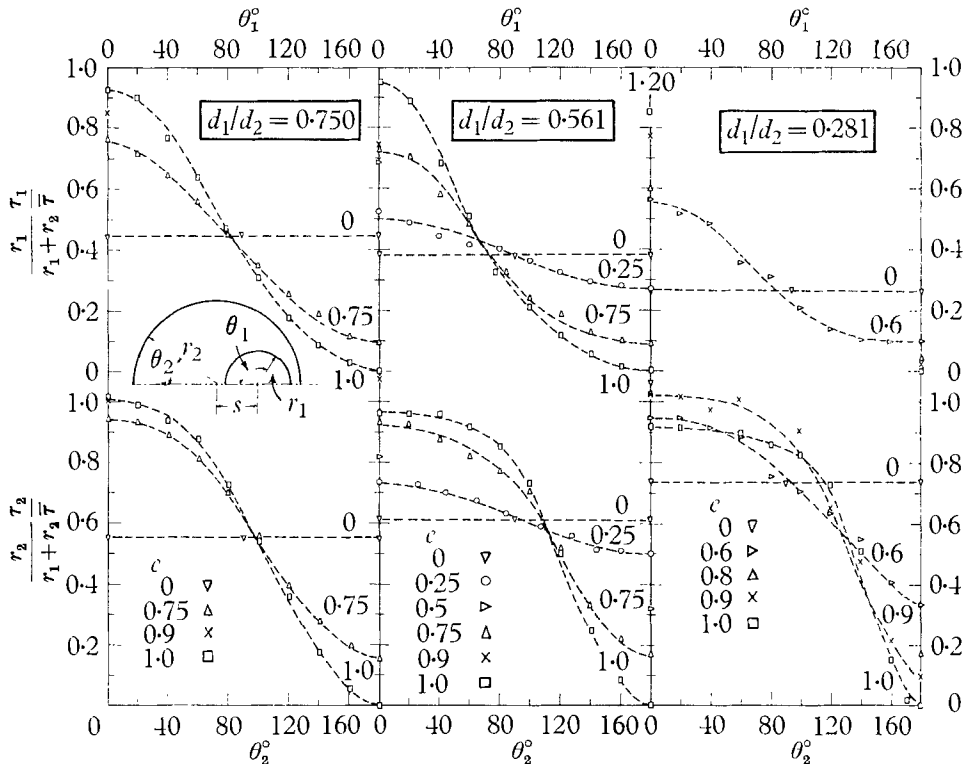

FIGURE 3. Circumferential distributions of local wall shear stress.

A presentation of the local shear stress results is made in figure 3. The figure consists of three graphs, respectively for $d_1/d_2 = 0.750$, 0.561, and 0.281. In turn, each graph is subdivided into an upper and lower part, in which are plotted results for the inner and outer bounding walls. For clarity, data points corresponding to a given eccentricity are connected by broken lines. For a few cases, the wall shear was determined only at $\theta = 0°$ and $180°$; these results are plotted as isolated points along the ordinate axes. The inset of the figure shows dimensional nomenclature and co-ordinates, particularly the angles θ_1 and θ_2.

Inspection of the figure shows that, for all the eccentric annular ducts investigated, there is a substantial circumferential variation of the wall shear. The largest shear values occur at the location of the widest gap ($\theta_1 = \theta_2 = 0°$), while the smallest values of the shear occur at the smallest gap ($\theta_1 = \theta_2 = 180°$). The distribution of the local shear stress decreases monotonically as θ_1 or θ_2 varies from 0° to 180°. Further study of the figure shows that, as d_1/d_2 decreases, there is a tendency for the τ_2 distribution to become more uniform in the range of small θ_2 values, especially at larger eccentricities. Correspondingly, but to a lesser extent, the variation of τ_1 tends to become steeper at small θ_1.

The data points for the 0·281 diameter-ratio duct show somewhat more scatter than do those for the other ducts; in addition, some shear-stress distributions along the inner wall were not determined. As will be discussed later, the shape of the velocity contour lines adjacent to the inner wall of the 0·281 diameter-ratio duct suggests the presence of a secondary flow at the higher eccentricities. Under secondary flow conditions, the gradient lines can no longer be regarded as lines of zero shear. Consequently, the force balance expressed by equation (4) no longer applies. The secondary flow adjacent to the inner wall may affect the flow pattern near the outer wall, thereby giving rise to the scatter noted above.

It is interesting to compare the magnitude of the shear on the inner wall to that on the outer wall. For instance, consideration may be given to $(\tau_1)_{\max}$ and $(\tau_2)_{\max}$, respectively at $\theta_1 = 0°$ and $\theta_2 = 0°$. In making such a comparison, cognizance should be taken of the factors $r_1/(r_1 + r_2)$ and $r_2/(r_1 + r_2)$ that multiply the ordinates of figure 3. It is readily verified that $(\tau_1)_{\max}/(\tau_2)_{\max} > 1$ for both concentric and eccentric ducts, with larger values corresponding to the latter. The magnitude of this ratio increases sharply as d_1/d_2 decreases.

5. The velocity field

In order to provide the broadest possible perspective, information on the velocity field is presented in three different ways. The first is in the form of contour maps, while the second and third show profiles along lines normal to the bounding walls, expressed either in terms of law-of-the-wall variables or defect-law variables.

5.1. *Contour diagrams*

The contour maps of figures 4 (*a*) and (*b*) have already been briefly alluded to. These are representative of a larger number of such diagrams that were prepared during the execution of this investigation; the complete set is available in Jonsson (1965). The contour diagrams were constructed from information obtained from velocity traverses normal to each of the bounding walls.

Figure 4 (*a*) shows the flow field for intermediate eccentricities for each of the three annular ducts, while figure 4 (*b*) pertains to the case $e = 1$. Aside from d_1/d_2 and e, each diagram is labelled with the corresponding values of the Reynolds number and ratio of the maximum to the bulk velocity, $u_{\max}/u_b$. The quantity $u_{\max}$ is the absolute maximum velocity in the duct cross-section; in general, this occurs along the line $\theta_1 = \theta_2 = 0$.

Each contour diagram is, in fact, a layout of the duct cross-section on which have been drawn lines of constant velocity (isovels). Each isovel represents a particular value of u/u_{max}. The use of dimensionless values for the contour lines
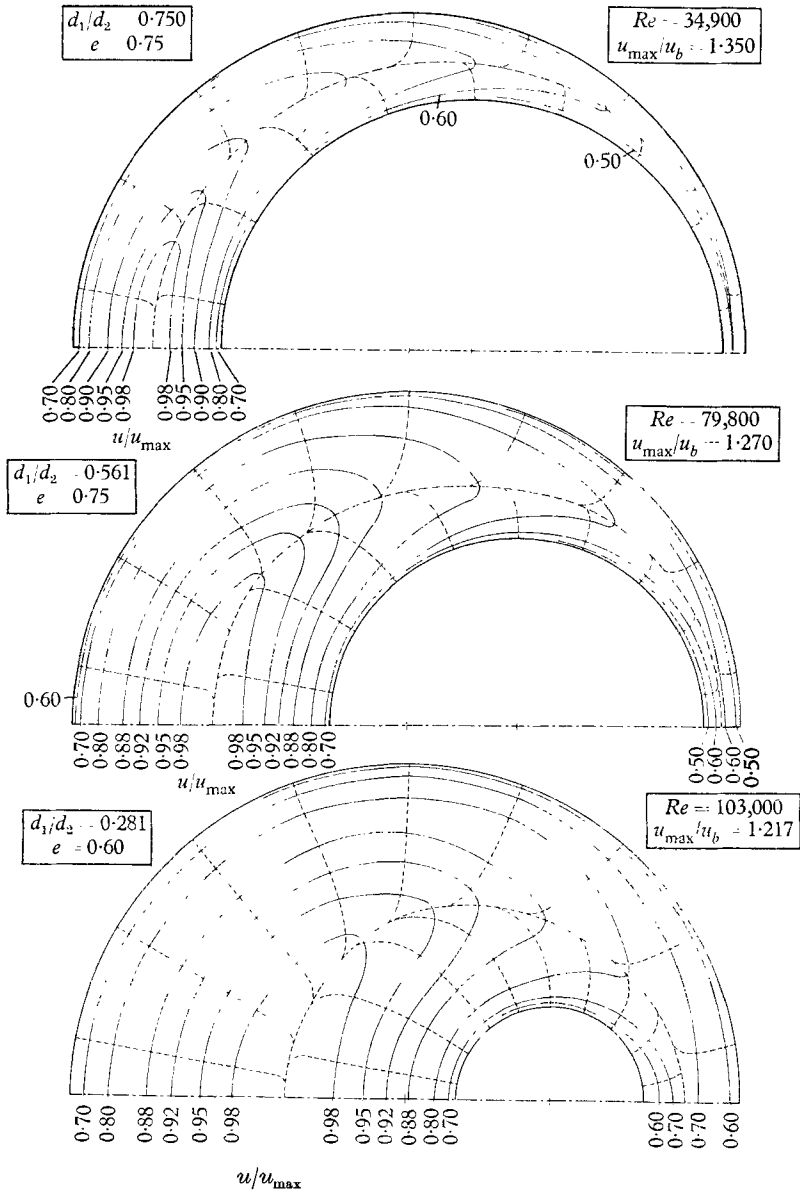
FIGURE (4a). Velocity contour diagrams.

acts to suppress the effect of Reynolds number. As already discussed, the broken lines were constructed normal to the isovels.

From figure 4 (*a*), it is seen that there are two types of contour lines characteristic of $0 < e < 1$: those that bound an area which lies completely within the flow, and those that bound an area that includes the inner tube. The former lines

correspond to the higher velocities and are concentrated in the widest part of the cross-section. The latter correspond to lower velocities and are found in the narrower part of the cross-section and along the walls of the wide part.
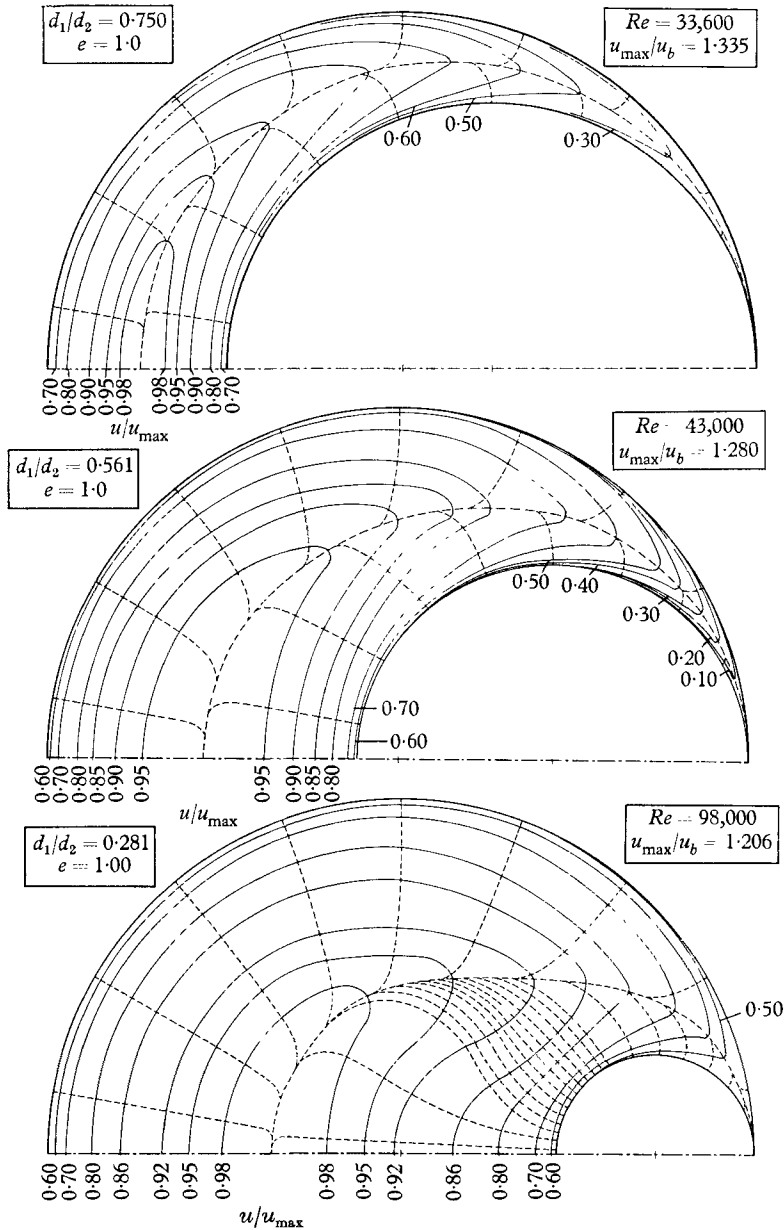

FIGURE 4(b). Velocity contour diagrams.

In annular ducts with an eccentricity of one, only the former type of contour lines appear (figure 4(b)). In the narrower part of the cross-section, the velocities are only a small fraction of those in the wide part. This suggests the possibility that laminar flow may exist in the narrow part of highly eccentric

annular ducts, while the flow in the remainder of the cross-section is turbulent. Such a phenomenon has been observed by Eckert & Irvine (1955) in triangular ducts.

Particular consideration may now be given to the contour diagram for

$$d_1/d_2 = 0{\cdot}281 \quad \text{and} \quad e = 1{\cdot}0$$

in figure 4 (*b*). It is seen that, by proceeding clockwise from the symmetry axis along a given contour line in the inner part of the flow, one moves inward toward the inner bounding wall. Correspondingly, the gradient lines are inverse S-shaped. These characteristics are altogether different from those of the other contour diagrams. It is the opinion of the authors that the distortion of the contour lines is due to secondary flow. A similar pattern was observed in the contour map for $d_1/d_2 = 0{\cdot}281$ and $e = 0{\cdot}9$.

5.2. *Law-of-the-wall velocity profiles*

It is common practice to represent turbulent velocity profiles for tube flow in terms of the so-called universal velocity distribution or law of the wall. Apart from the laminar sublayer and buffer regions, which are confined to the immediate neighbourhood of the wall, the universal velocity distribution is logarithmic in form, that is

$$u^+ = A \ln y^+ + B, \tag{7}$$

in which

$$u^+ = u/u_\tau, \quad y^+ = y u_\tau/\nu, \quad u_\tau = \sqrt{(\tau/\rho)}. \tag{8}$$

In the foregoing, y is the distance from the wall as measured along a line normal to the wall, and τ is the wall shear at the point from which y is measured. The quantity u_τ is frequently called the friction velocity. The form of equation (7) has been derived by a number of authors, two of the earliest being Prandtl and von Kármán.

In their analysis of turbulent flow in an eccentric annular duct, Deissler & Taylor assumed that the law of the wall continued to be valid when applied along lines perpendicular to the walls of the annulus. τ was interpreted as the *local* wall shear at the point at which the perpendicular is erected. The constants A and B employed by Deissler & Taylor were 2·78 and 3·8, respectively.

The traversing mechanism of the present investigation was designed to permit measurement of velocity profiles along lines perpendicular to either bounding wall of the duct. When taken together with the previously discussed distributions of local wall shear, these measurements can be represented in terms of the u^+, y^+ variables of the law of the wall. A presentation of the measured velocity profiles in terms of the law-of-the-wall variables is made in figures 5 through 8. The first of these figures contains information for the case of the concentric annulus for all three duct diameter ratios, while figures 6, 7, and 8 respectively correspond to the eccentric annular ducts with diameter ratios of 0·750, 0·561, and 0·281.

Consideration may first be given to the concentric case, figure 5. The left-hand portion of the figure pertains to the outer velocity profile; correspondingly, τ_2 is the shear stress on the outer wall and y_2 is the distance from the outer wall,

measured along a perpendicular. The right-hand part of the figure is for the inner velocity profile; and τ_1 and y_1, respectively, denote the shear stress on the inner wall and the distance measured perpendicular to the inner wall. The plotted data not only include all three diameter ratios, but also a range of Reynolds numbers. As expected, the latter does not appear to be a significant factor in the u^+, y^+ presentation.
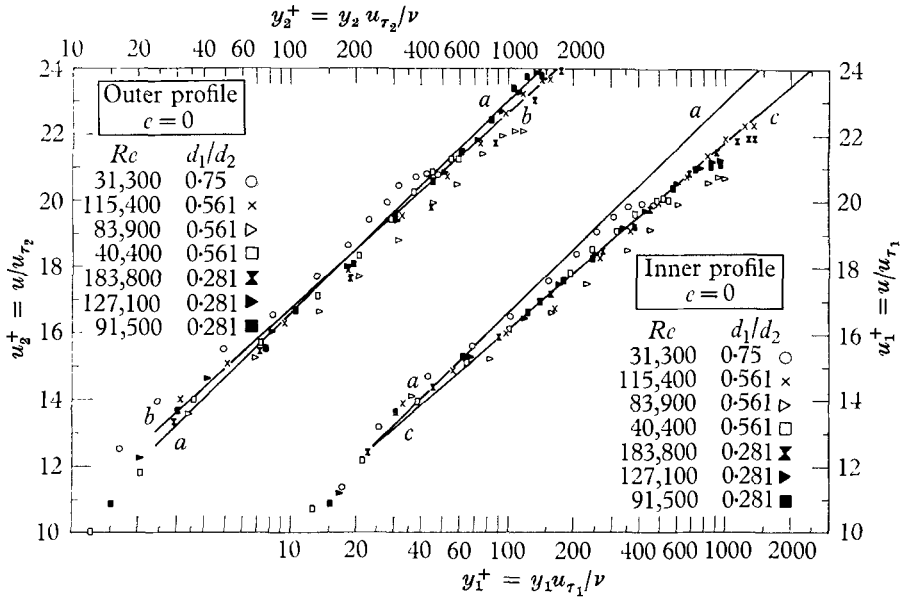

FIGURE 5. Law-of-the-wall velocity profiles, concentric annuli.

The various straight lines that appear in the figure represent the following expressions

$$aa \quad u^+ = 2{\cdot}78 \ln y^+ + 3{\cdot}8; \tag{9a}$$

$$bb \quad u^+ = 2{\cdot}56 \ln y^+ + 4{\cdot}9; \tag{9b}$$

$$cc \quad u^+ = 2{\cdot}44 \ln y^+ + 4{\cdot}9. \tag{9c}$$

The line aa corresponds to that of the Deissler–Taylor analysis, while bb and cc are mean lines drawn through the data for the outer and inner profiles.

By inspection of the figure, it is seen that the Deissler–Taylor line is in good agreement with the measured outer profiles. In the case of the inner profile, the analytical line falls somewhat above the data, but the agreement is still satisfactory. A similar finding has been reported by Brighton & Jones (1964). The fact that the standard universal velocity distribution is not a fully adequate representation of the inner profile is readily understood when it is realized that the flow along the inner tube is quite similar to the *external* flow longitudinal to a cylinder. It has been demonstrated by Sparrow, Eckert & Minkowycz (1963) that the effect of transverse curvature is to produce a lower u^+ at a given y^+.
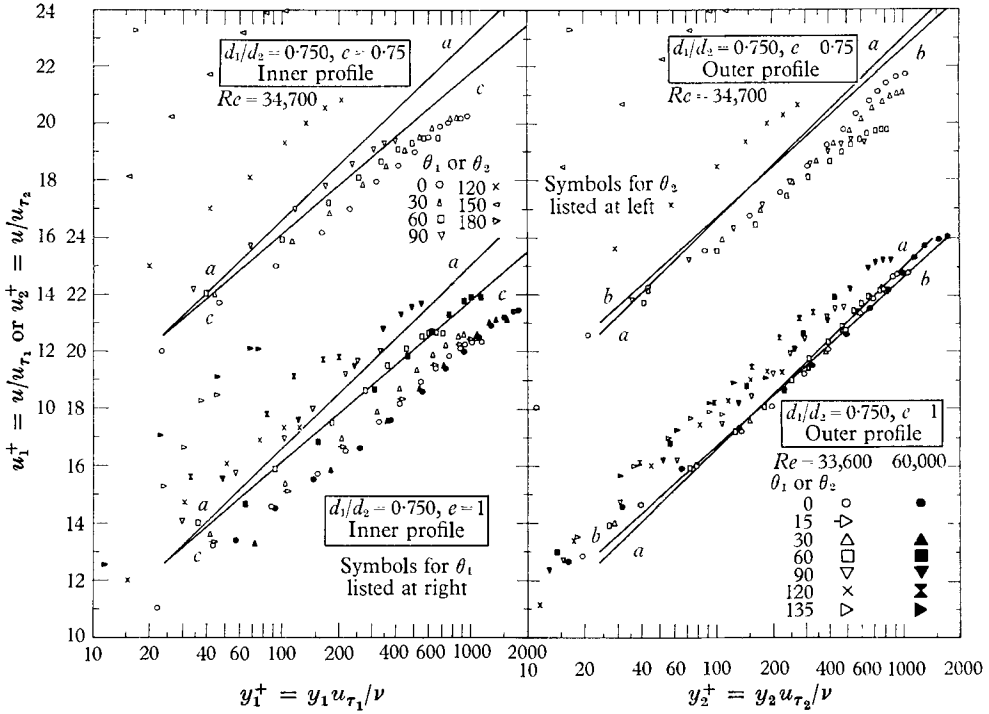
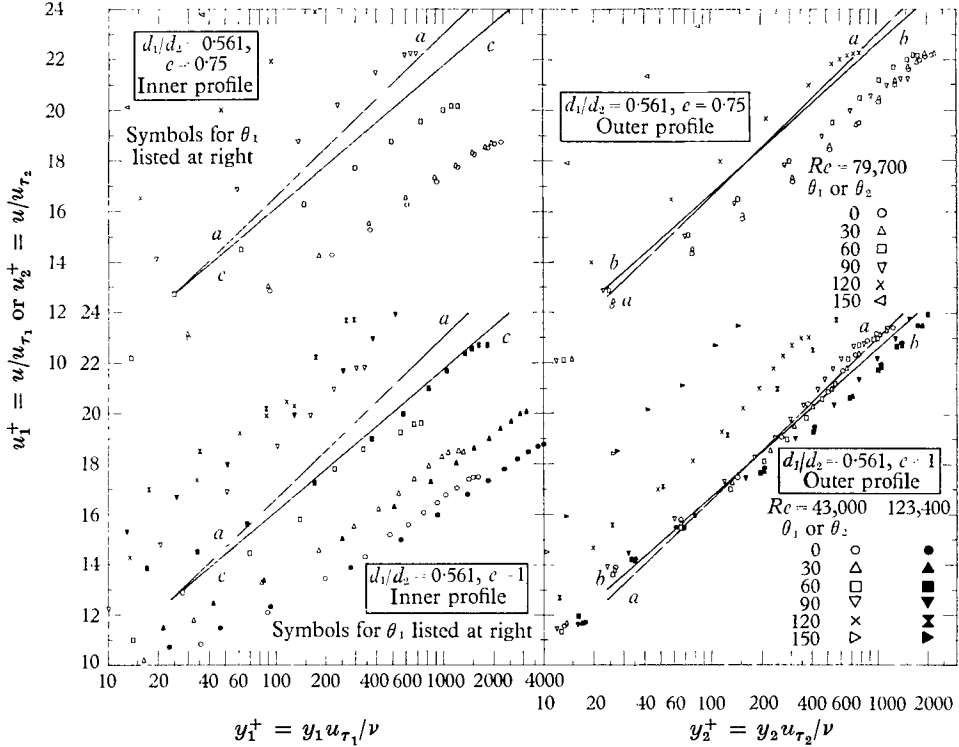FIGURE 6. Law-of-the-wall velocity profiles, eccentric annuli, $d_1/d_2 = 0.750$.

FIGURE 7. Law-of-the-wall velocity profiles, eccentric annuli, $d_1/d_2 = 0.561$.

$$y_1^+ = y_1 u_{\tau_1}/\nu \qquad\qquad y_2^+ = y_2 u_{\tau_2}/\nu$$

Symbols for θ_1 listed at right

$d_1/d_2 = 0.281,\ c = 0.6$
Inner profile

$d_1/d_2 = 0.281,\ c = 0.6$
Outer profile
$Re = 103,000$

θ_1 or θ_2

0	○	120	×
30	△	150	▷
60	□	180	◁
90	▽		

$d_1/d_2 = 0.281,\ c = 1$
Outer profile
$Re = 96,600\quad 149,400$

0	○		●
30			▶
60	△		▲
90	□		■
120	▽		▼
150	×		

$d_1/d_2 = 0.281,\ c = 0.9$
Outer profile
$Re = 98,860$

0	○	90	▽
30	△	120	×
60	□	150	◁

$u_1^+ = u/u_{\tau_1}$ or $u_2^+ = u/u_{\tau_2}$

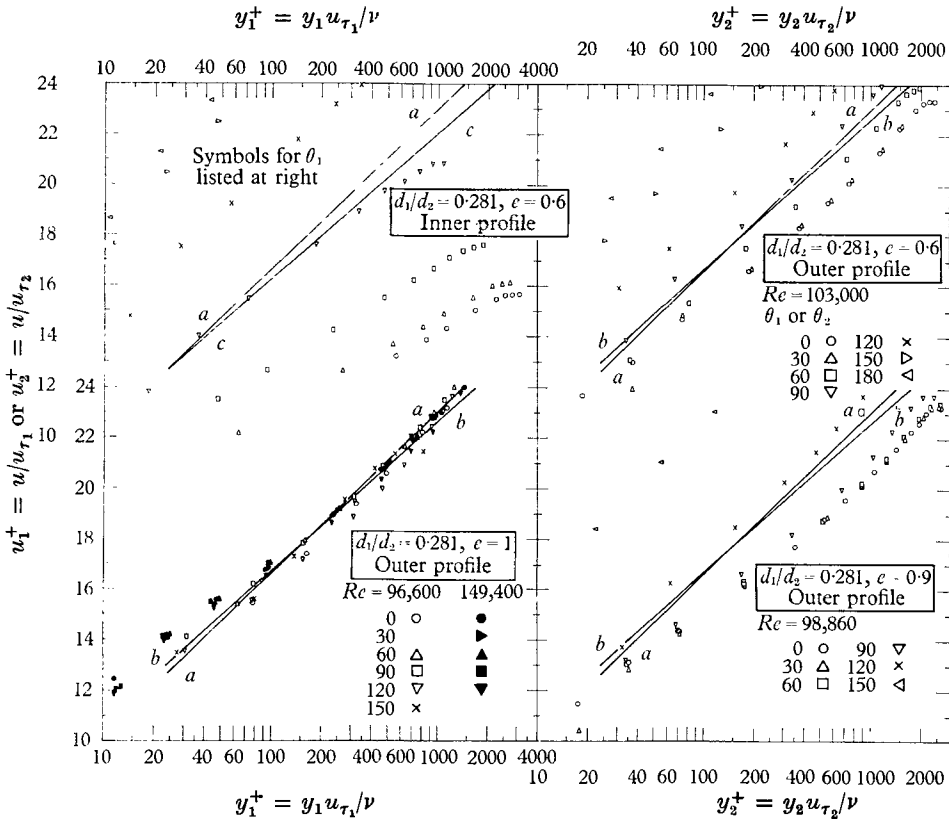$$y_1^+ = y_1 u_{\tau_1}/\nu \qquad\qquad y_2^+ = y_2 u_{\tau_2}/\nu$$

FIGURE 8. Law-of-the-wall velocity profiles, eccentric annuli, $d_1/d_2 = 0.281$.

Attention may now be directed to the results for the eccentric annular ducts, figures 6, 7, and 8. Each of these figures includes four groupings of data. In figures 6 and 7, two groups of inner profiles are shown in the left-hand portion and two groups of outer profiles are shown in the right-hand portion. In figure 8 there are three groups of outer profiles and one group of inner profiles.† The lines aa, bb, and cc, which represent equations $(9a)$, $(9b)$, and $(9c)$, are included for purposes of reference.

The data points appearing in these figures are parameterized by the angles θ_1 or θ_2 for the inner or outer profiles, respectively. As illustrated in the inset of figure 3, these angles specify circumferential locations along the inner and outer walls. Data corresponding to a fixed value of θ_1 represent a traverse along a normal to the inner wall at the location θ_1; τ_1 is the *local* shear stress at θ_1, and y_1 is the distance measured normal to the inner wall. Similarly, data corresponding to a fixed value of θ_2 correspond to a traverse normal to the outer wall at the location θ_2, with τ_2 and y_2 respectively denoting the *local* shear at θ_2 and the distance measured normal to the outer wall.

† As previously noted, the presence of secondary flow prevented the determination of the local shear distribution on the inner wall at the higher eccentricities for the $d_1/d_2 = 0.281$ duct.

An overall appraisal of these figures suggests the following general remarks. For the outer profiles there is fair agreement between the data and the universal velocity distribution (line aa) when θ_2 is no larger than 90° or 120°. At larger angles, the experimental points lie significantly higher than the universal line. For the inner profile, similar remarks apply for the largest diameter-ratio duct, $d_1/d_2 = 0.750$. However, for the intermediate and smallest diameter-ratio ducts, there appears to be little similarity between the data and the universal distribution.

In light of the information appearing in figures 6 to 8, it appears that the measurements do not substantiate the assumption that the universal velocity distribution is valid along all lines normal to the bounding walls. Yet, not-withstanding this, the friction factors predicted by analysis were found to be in fair agreement with those of experiment. It is well to remember, however, that the friction factor is an overall quantity, the computation of which may tend to iron out local deficiencies of the analytical model.

5.3. *Defect-law profiles*

An alternative representation of turbulent pipe-flow information is the velocity defect law. The most general form of the defect law for pipe flows, recently stated by Hinze (1959), is

$$(u_m - u)/u_\tau = -2.44 \ln (y/\Delta) + 0.8 + h(y/\Delta), \tag{10}$$

in which $h(y/\Delta)$ is a correction factor that may be taken from figure 7–30 of the aforementioned reference. In (10), Δ is the distance between the wall and the point at which a velocity maximum is achieved as one moves along a normal to the wall; u_m is the value of the maximum velocity; u_τ is the friction velocity ($= \sqrt{(\tau/\rho)}$) as previously discussed.

The measured velocity profiles of the present investigation have been phrased in terms of defect-law variables and are plotted in figures 9 through 12. The first of these figures is for the concentric annulus, while the remainder are for the eccentric annulus. Specifically, figures 10, 11 and 12 respectively correspond to the duct diameter ratios of 0.750, 0.561, and 0.281. Each figure contains several groupings of data. For purposes of reference, the pipe-flow correlation of Hinze, equation (10), has been drawn through each grouping. In some cases, data for a range of Reynolds numbers have been plotted together. No significant difference was observed for these various Reynolds numbers.

Figure 9 is subdivided into three parts respectively for each of the three concentric annuli. The ordinate quantities u_{τ_1} and u_{τ_2} are referred to the corresponding shear stresses τ_1 and τ_2 on the inner and outer walls. The abscissa quantities Δ_1 and Δ_2 are the respective normal distances from the inner and outer walls to the location of maximum velocity. u_m is the magnitude of the maximum velocity. From the figure, it is seen that there is very good agreement between the data for the outer velocity profile and the Hinze defect law. The measured inner velocity profile tends to fall somewhat below the defect law. This finding is similar to that encountered in the law-of-the-wall representation, and the same explanation applies.
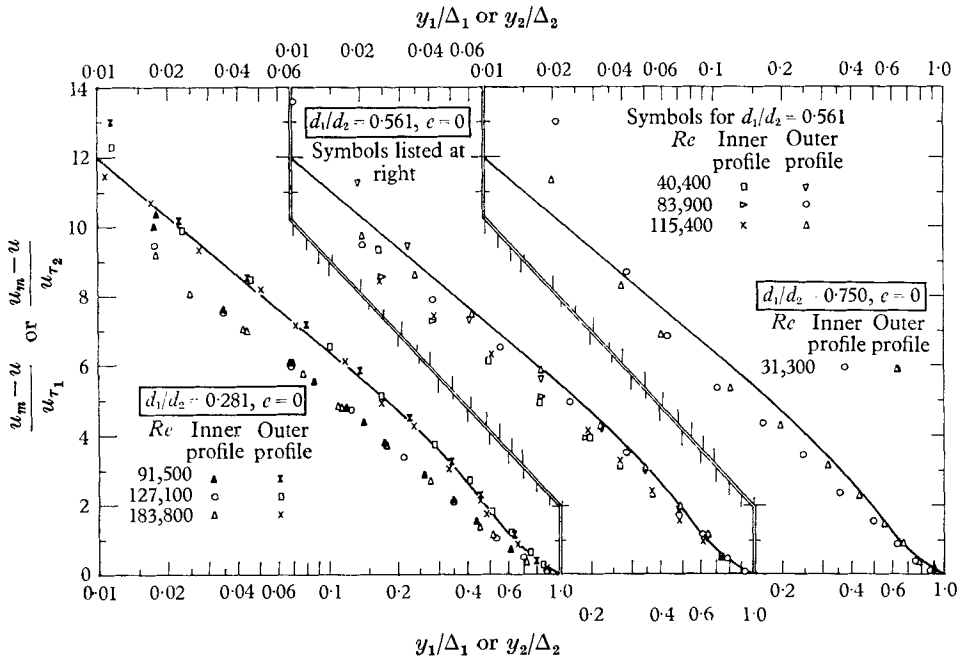
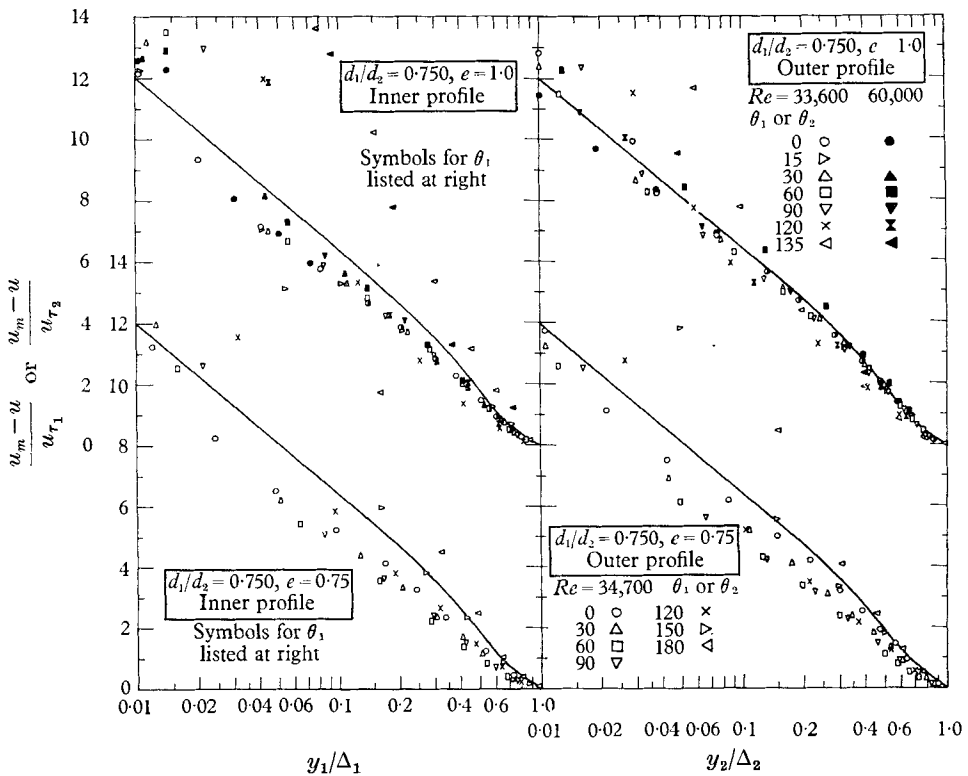FIGURE 9. Defect-law profiles, concentric annuli.

FIGURE 10. Defect-law profiles, eccentric annuli, $d_1/d_2 = 0.750$.

The results for the eccentric annuli, as presented in figures 10, 11, and 12, may now be considered. In these figures, the data points are parameterized by the angles θ_1 and θ_2 that represent circumferential locations on the inner and outer bounding walls, respectively. For a given value of θ_1, u_m is the maximum velocity that is encountered as one moves normal to the inner wall at that θ_1;
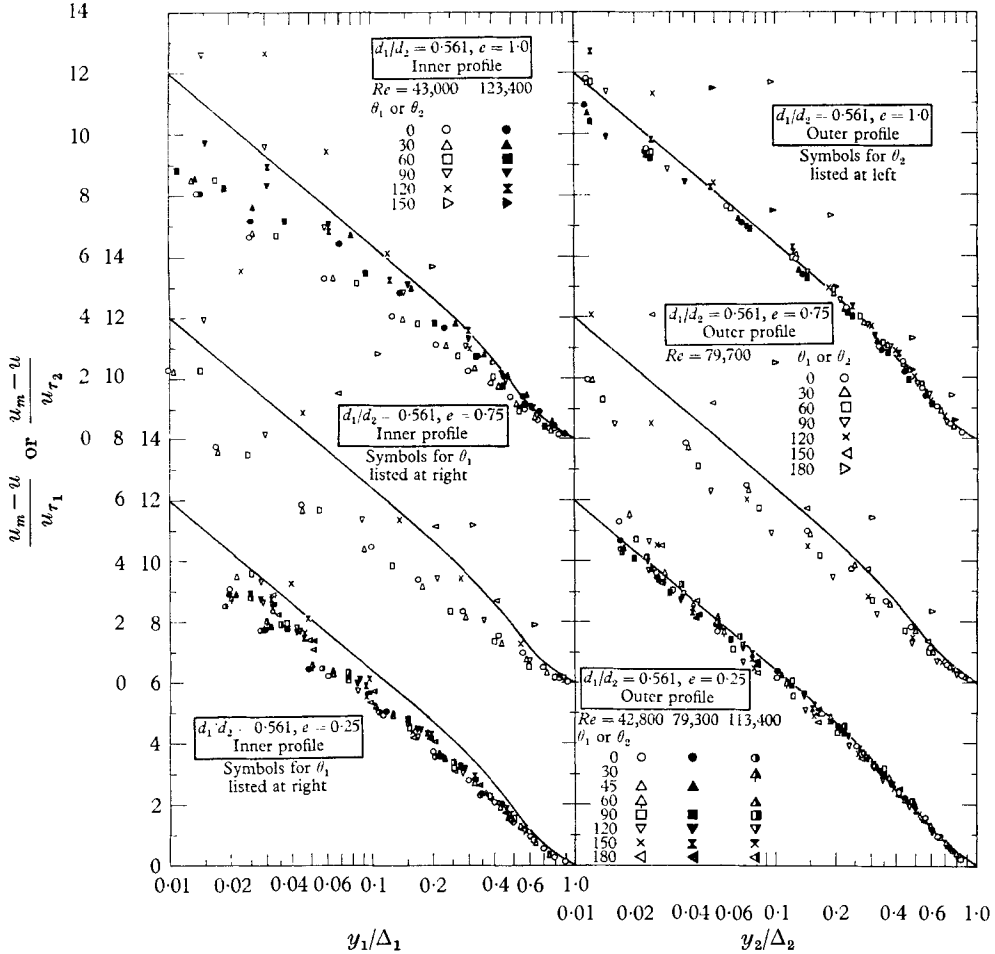

FIGURE 11. Defect-law profiles, eccentric annuli, $d_1/d_2 = 0.561$.

correspondingly Δ_1 is the distance from the wall to the location of the maximum. Thus both u_m and Δ_1 are specific for the given θ_1. Furthermore, u_{τ_1} corresponds to the local wall shear. Data points labelled with the same value of θ_1 represent a traverse normal to the inner wall, with y_1 denoting the distance from the wall. For a fixed value of θ_2, the quantities u_m, Δ_2, u_{τ_2}, and y_2 are similarly interpreted.

It is seen from the figures that there is good overall agreement between the data for the outer profiles and the defect law. The agreement is especially good for the smallest diameter ratio (figure 12) and at both small and large

eccentricities for the other diameter ratios (figures 10 and 11). However, for the latter diameter ratios, the agreement for the intermediate case $e = 0.75$ is not quite as good. Closer inspection of the figures shows that, in some instances, there are significant departures of the data from the defect law at larger values of θ_2 and at smaller values of y_2/Δ_2. However, the defect law itself is not meant to hold at very small distances from the wall.

The correlation of the inner profile with the defect law is not quite as good as that just discussed for the outer profile. For the largest diameter-ratio duct as well as for the intermediate diameter-ratio duct with the smallest eccentricity
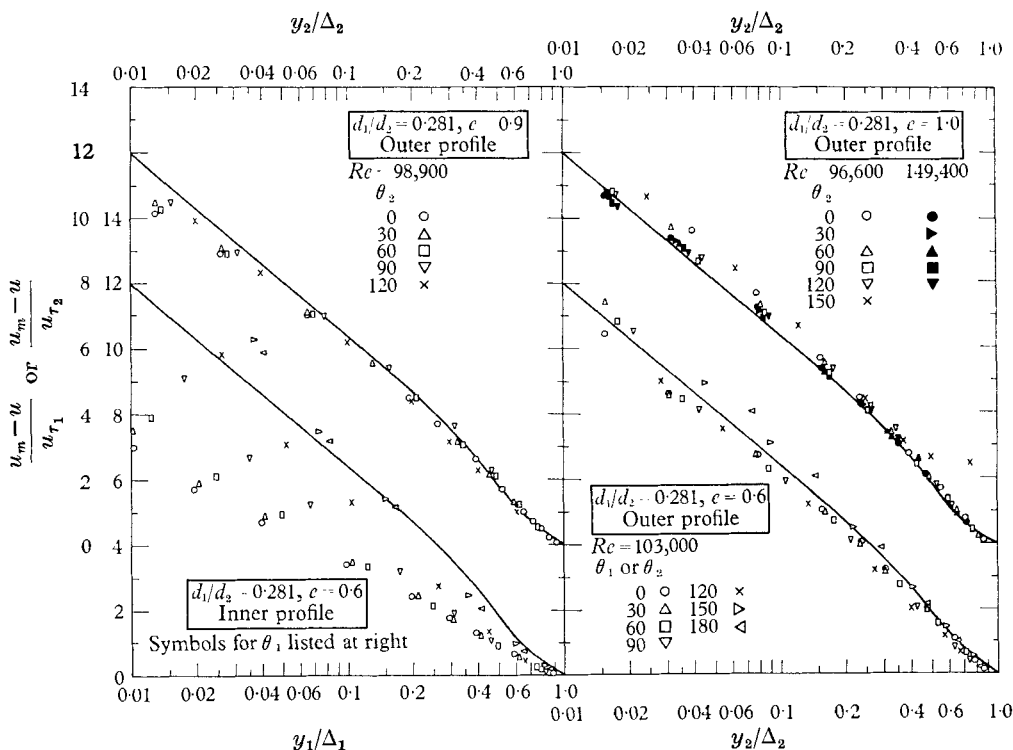

FIGURE 12. Defect-law profiles, eccentric annuli, $d_1/d_2 = 0.281$.

($e = 0.25$), the extent to which the inner and outer profiles correlate with the defect law is not too different. However, for the other cases, there are greater differences in the extent of the correlation. In general, the data points for the inner profile tend to lie lower than the curve at small and intermediate values of θ_1, especially at smaller diameter ratios. This could well be due to the transverse curvature effect previously mentioned.

When the law-of-the-wall and the defect-law representations of the data are compared, it appears that the latter agrees better with standard tube-flow correlations than does the former. However, the use of the defect law requires a knowledge of the magnitude and the location of the maximum velocity along a line normal to the wall, in addition to the local wall shear. Only the latter is needed for the application of the law of the wall.

6. Hydrodynamic entrance length and circumferential pressure variation

In an earlier section of this paper, it was mentioned that pressure-gradient information had been obtained for the hydrodynamic development region as well as for the fully-developed régime. Space limitations preclude graphical presentation of the axial pressure gradients here.† For present purposes, it is believed to be particularly relevant to report hydrodynamic entrance lengths that have been deduced from these pressure gradients. A knowledge of the length required for hydrodynamic development is essential for the proper application of fully-developed results.

d_1/d_2	e			
	0.0	0·5	0·9	1·0
0·281	29	32	38	38
0·561	26	38	59	78
0·750	28	50	69	91

TABLE 1. Entrance length, z/d_h (2 % approach to fully-developed pressure gradient)

The hydrodynamic entrance length will be defined here as the distance from the duct inlet that is required for the pressure gradient to approach to within 2 % of the fully-developed value. Table 1 lists these entrance lengths in terms of the hydraulic diameter d_h. From the table, it is seen that, for any fixed duct diameter ratio, the entrance length increases with increasing eccentricity. At small values of d_1/d_2, the effect of eccentricity is relatively minor. However, when d_1/d_2 is large, the eccentricity has a decisive effect. For instance, for $d_1/d_2 = 0.75$, the development length for a duct of unit eccentricity is about three times that for the concentric duct. In light of the information presented in table 1, it appears that the pressure measurements of Dodge (1963) might well have been affected by the entrance region.

In planning this investigation, it was felt that some indication of the relationship between the non-axisymmetric flow field and the circumferential pressure variation, if any, would be of interest. To this end, six circumferentially arranged pressure taps were installed at each of four axial locations on the outer tube. Representative information obtained from such measurements is presented in table 2. At each axial station, the tabulated quantity is the difference in pressure between the positions $\theta_2 = 0$ and $\theta_2 = \theta_2$, expressed in inches of water.

These data correspond specifically to a duct diameter ratio of 0·561 and to eccentricities of zero and one. For this diameter ratio, the measurement stations are at 10, 30, 60, and 100 hydraulic diameters from the inlet of the duct. In the concentric case, the last two stations fall within the fully-developed region, while, for the fully eccentric case, only the last station can be so regarded. The fully-developed longitudinal pressure gradients, dp/dz, were 0.39 and 0·33 in.

† Interested readers may consult Jonsson (1965).

of water/ft. for the eccentricities of zero and one, respectively. The internal circumference of the outer tube is approximately 12·5 in.

It may be observed from the table that a circumferential pressure variation was detected even in the case of the concentric annulus. Considering the somewhat irregular nature of the variation, it is reasonable to suspect slight local

θ_2	$z/d_h = 10$		$z/d_h = 30$	
	$e = 0$	$e = 1$	$e = 0$	$e = 1$
0	0·000	0·000	0·000	0·000
90	0·006	0·006	0·005	0·007
150	−0·006	−0·035	0·005	−0·004
180	−0·006	−0·014	0·007	−0·022
210	−0·003	−0·044	0·006	−0·003
270	−0·002	0·004	0·005	0·006
θ_2	$z/d_h = 60$		$z/d_h = 100$	
	$e = 0$	$e = 1$	$e = 0$	$e = 1$
0	0·000	0·000	0·000	0·000
90	0·006	0·006	−0·002	−0·003
150	0·002	−0·009	0·002	−0·012
180	0·002	−0·012	−0·003	−0·011
210	0·004	−0·007	−0·002	−0·010
270	0·002	0·003	0·000	−0·003

TABLE 2. Circumferential pressure variation: $d_1/d_2 = 0.561$; $Re \approx 100,000$; $p(\theta_2) - p(0)$, inches of water

differences in pressure-tap geometry. However, it is noteworthy that the pressure variations do diminish at larger z/d_h. This suggests that there might be a slight flow asymmetry in the entrance region that decays with increasing downstream distance.

Attention may now be focused on the results for the eccentric annulus. Specifically, at the fully-developed station $z/d_h = 100$, it is seen that the circumferential pressure variation is quite regular and is substantially larger than that for the concentric annulus. The effect of such a circumferential pressure variation on the flow pattern cannot be stated with certainty. However, it may be noted that the velocity contour maps for this case contain no irregularities suggestive of a secondary flow. Furthermore, the longitudinal pressure gradient did attain a constant fully-developed value. On this basis, one may conclude that the flow pattern was not affected in a fundamental way.

REFERENCES

BRIGHTON, J. A. & JONES, J. B. 1964 Fully developed turbulent flow in annuli. *J. Basic Engineering*, D **86**, 835.

DEISSLER, R. G. & TAYLOR, M. F. 1955 Analysis of fully developed turbulent heat transfer and flow in an annulus with various eccentricities. *NACA TN* no. 3451.

DODGE, N. A. 1963 Friction losses in annular flow. *The American Society of Mechanical Engineers*, paper no. 63-WA-11.

ECKERT, E. R. G. & IRVINE, T. F. 1955 Simultaneous turbulent and laminar flow in ducts with noncircular cross-sections. *J. Aero. Sci.* **22**, 65.

HINZE, J. O. 1959 *Turbulence*. New York: McGraw-Hill.

JONSSON, V. K. 1965 Experimental studies of turbulent flow phenomena in eccentric annuli. Ph.D. Thesis, University of Minnesota, Minneapolis, Minnesota.

SPARROW, E. M., ECKERT, E. R. G. & MINKOWYCZ, W. J. 1963 Heat transfer and skin friction for turbulent boundary-layer flow longitudinal to a circular cylinder. *J. App. Mech.* E **30**, 37.

WOLFFE, R. A. 1962 Axial turbulent flow in a circular pipe containing a fixed eccentric core. M.S. Thesis, Lehigh University, Bethlehem, Pennsylvania.